Cross-Sensitivity of a Dual-Port Potentiometric Sensor based on Auto-Tuning RFID ICs

Francesca M. C. Nanni
IEEE Student Member
University of Rome Tor Vergata
Email: frmach97@gmail.com

Nicoletta Panunzio
IEEE Student Member
University of Rome Tor Vergata
Email: nicoletta.panunzio@uniroma2.it

Gaetano Marrocco
IEEE Senior Member
University of Rome Tor Vergata
Email: gaetano.marrocco@uniroma2.it

***Abstract*—Skin monitoring devices, like Ultra-High-Frequency (UHF) Radio Frequency Identification (RFID) Epidermal sensors, can improve Point of Care (PoC) testing, with benefits such as faster and more accurate diagnoses, improved patient outcomes, and increased convenience. Since a comprehensive screening of the user/patient may require the simultaneous acquisition of multiple parameters, the cohabitation of several wireless sensors in a small space will be highly likely in the near future. This will, however, force proximity of the antennas and their Integrated Circuits (ICs), leading to coupling interactions, that are typical of multi-sensing systems. This paper introduces a model that evaluates the cross-sensitivity, i.e., the mutual interference, of a system of two RFID-coupled sensors, preliminarily evaluated off-skin. The model specifically involves a peculiar class of RFID ICs equipped with auto-tuning technology that offered up new sensing opportunities in recent years. The mathematical relationships governing the coupling phenomenon are derived and then numerically implemented for different coupling arrangements. Our promising results, corroborated by experimental evaluations, reveal that configurations with very low cross-sensitivity can be achieved, suggesting the feasibility of designing a device capable of simultaneously monitoring multiple potentiometric parameters without any interference between close ICs.**

***Keywords*—point of care, RFID, electromagnetic coupling, self-tuning technology, cross-sensitivity.**

I. Introduction

Point of Care (PoC) testing and procedures can lead to faster, more accurate diagnoses and treatments, improved patient outcomes, reduced costs, increased convenience and accessibility [1]. In particular, PoC-based on skin monitoring devices can be used to measure a variety of physiological parameters and are best suitable for medical diagnostics. Devices that, for example, sense blood levels of both glucose and lactate can be used for people with diabetes [2]. They can hence provide real-time monitoring and help patients and doctors managing their condition more effectively.

Battery-free on-skin devices have been proposed recently and the acquisition, processing, and transmission of sensor data are operated by an electromagnetic device equipped with an antenna, a chemical sensor, and a transponder Integrated Circuit (IC). In particular, the newest developments in Radio Frequency Identification (RFID) technology are promoting the establishment of a class of bio-integrated skin devices that take advantage of low-power and passive wireless communication and sensing interfaces [3], [4] with the additional benefits of low-cost and disposability.

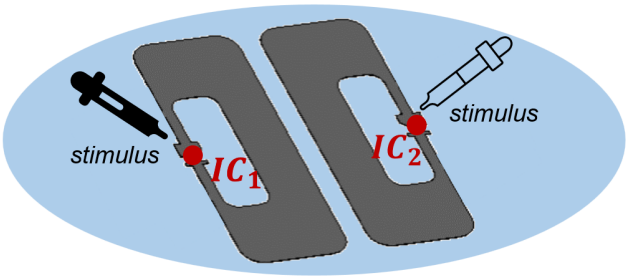

Fig. 1. Concept figure of a closely coupled sensor system.

Since accurate sensing of the user/patient requires the simultaneous acquisition of multiple parameters, the cohabitation of several wireless sensors in a small space will be inevitable shortly. This condition forces the proximity of the antennas and ICs, leading to coupling interactions, that are typical of multi-sensing systems.

The main challenge for the reliable operation of such systems will hence be the evaluation of the cross-talk, i.e., the interference of one signal with another [5], which can lead to inaccurate measurements and misinterpretation of data. Also, the calibration of sensors may become challenging to manage, since the presence of one sensor may affect the calibration of others.

The evaluation of multi-sensing performance requires an in-depth investigation of "cross-sensitivity", induced by electromagnetic coupling, since it can otherwise lead to false readings and inaccurate measurements.

By extending the results presented in [6] and [7], this paper aims to introduce a model that evaluates the cross-sensitivity of a system of two RFID-coupled sensors (Fig. 1). We rely on auto-tuning ICs, which can autonomously adjust their internal RF admittance to make IC-antenna matching rather insensitive to changes in the local boundary conditions. A general theoretical electromagnetic model of auto-tuning RFID ICs has been presented in [8] in the case of a single-chip device, further developed in [9] in the case of near-field reader-to-tag communication, and fully exploited by the interface with external potentiometric sensors [6]. Here we propose an

electromagnetic model of the cross-sensitivity of the two-port sensing device and we quantify the effect of coupling in some reference examples.

This paper is organized as follows: Section II extends the auto-tuning model to the case of coupled RFID antennas [10]. In Sections III and IV, the theoretical findings are then numerically and experimentally verified using a reference couplet of sensors in various arrangements.

II. Methodology

A. Sensing architecture

The reference dual port system, with functional modules of the sensing architecture and the corresponding interactions, is sketched in Fig. 2.

Let us consider two external stimuli $\mathbf{\Psi} = [\psi_1, \psi_2]$, separately interacting with each IC. Each stimulus is intended as any variable boundary condition that affects the *n-th* IC performance due to an alteration of the antenna-IC impedance matching with respect to an unperturbed reference condition. By means of potentiometric or capacitive sensors, stimuli will cause the variation of the capacitances $C_{S,n}$ interconnected in parallel with the antenna and the IC at each side of the network. This will induce a mismatch with the corresponding microchip's admittances.

B. Auto-tuning technology

If the connected IC is provided with auto-tuning technology, it can be modeled as an adaptive internal network of capacitors, where starting from a minimum value $C_{IC,0}$, the overall capacitance is modulated with incremental steps $C_{IC,step}$ such that:

$$C_{IC}(s_n) = C_{IC,0} + s_n C_{IC,step}. \tag{1}$$

The integer number "s_n", hereafter referred as *sensor code*, is returned by the IC at the *n-th* port following a standard RFID query. In this way, each auto-tuning inbuilt circuitry enables to dynamically adjust the IC susceptance to account for the fluctuating antenna susceptance, by enforcing that:

$$\left|B_{IC}(s_n) + B_n^{in}(\mathbf{\Psi})\right| = 0 \tag{2}$$

where $B_n^{in}(\mathbf{\Psi}) = B_{A,n} + \omega C_{S,n}$ is the input susceptance seen at the *n-th* microchip looking toward the antenna, also including the variable capacitance. $B_{IC}(s_n) = \omega C_{IC}(s_n)$ is instead the microchip susceptance.

By inverting (2), the retuning indicator s_n is found to be directly proportional to $B_n^{in}(\mathbf{\Psi})$:

$$s_n(\mathbf{\Psi}) = S_{min} + nint\left(\frac{-1}{C_{IC,step}}\left(C_{IC}(S_{min}) + \frac{B_n^{in}(\mathbf{\Psi})}{\omega}\right)\right). \tag{3}$$

The auto-tuning effort is generally limited so that the sensor code will vary within the range $S_{min} < s_n < S_{max}$, being S_{min} and S_{max} dependent on the implementation of the IC. In case of a more severe mismatch, the sensor code saturates to the nearest boundary value.

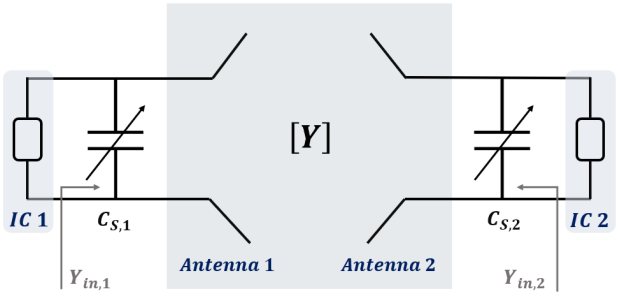

Fig. 2. Equivalent circuit of the dual sensing architecture.

C. Coupling

In case of electromagnetic coupling, the input susceptance of the *n-th* antenna is affected not only by the overall multi-device arrangement and the local environment, but also by the susceptance of the other ICs nearby.

Let $Y_{IC,n} = G_{IC,n} + jB_{IC,n}(s_n)$ denote the dynamic admittance of the IC at the *n-th* port. Overall, the port's terminations are accounted for by a diagonal matrix $\boldsymbol{Y_{IC}} = \boldsymbol{G_{IC}} + j\boldsymbol{B_{IC}} = \boldsymbol{diag}\left(\boldsymbol{Y_{IC,1}}, \boldsymbol{Y_{IC,2}}\right)$ and the general 2-port system collecting the interrogating electromagnetic field is modeled by the 2×2 admittance matrix $\mathbf{Y} = \mathbf{G} + j\boldsymbol{B}$.

From [7], the most general formula of the input admittance at the *n-th* port is:

$$Y_n^{in} = \sum_{m=1}^{2} Y_{nm} \frac{\left[\mathbf{Y_G^{-1}}\right]_{\mathbf{m}} \cdot \boldsymbol{g}}{\left[\mathbf{Y_G^{-1}}\right]_{\mathbf{n}} \cdot \boldsymbol{g}}, \tag{4}$$

where $\left[\mathbf{Y_G^{-1}}\right]_{\mathbf{n}}$ indicates the *n-th* row of the inverse of the system admittance matrix $\mathbf{Y_G} = \mathbf{Y} + \mathbf{Y_{IC}} + \mathbf{Y_{Cs}}$ and $\boldsymbol{g}$ is the column vector of the normalized radiation gains which groups the parameters of the system. Note that, in addition to the system and IC matrix $\boldsymbol{Y}$ and $\boldsymbol{Y_{IC}}$, the grid matrix $\mathbf{Y_G}$ also contains the diagonal matrix of the admittances of the variable capacitances placed in parallel to both ICs and antennas $\boldsymbol{Y_{Cs}} = \boldsymbol{G_{Cs}} + j\boldsymbol{B_{Cs}} = \boldsymbol{diag}\left(\boldsymbol{Y_{Cs,1}}, \boldsymbol{Y_{Cs,2}}\right)$.

It is worth noticing that the admittance matrix $\boldsymbol{Y_G}$ is influenced by both external boundary conditions and adaptive variations in each IC's admittance via the sensor codes $s_n(\mathbf{\Psi})$:

$$\mathbf{Y_G}(\mathbf{\Psi}) = \mathbf{Y} + \mathbf{Y_{IC}}(\boldsymbol{s}(\mathbf{\Psi})) + \mathbf{Y_{Cs}}(\mathbf{\Psi}) \tag{5}$$

where $\mathbf{s}(\mathbf{\Psi}) = [s_1(\Psi_1), s_2(\Psi_2)]$. As a result, the same entangled dependence holds true for the *n-th* port's input admittance $Y_n^{in}(\mathbf{\Psi})$.

Particular attention must be focused at Eq. (4) in which the input admittance now depends on both the external parameter $\mathbf{\Psi}$ and the sensor code $\boldsymbol{s}$ so that $Y_n^{in} = f(\Psi_1, \Psi_2, s_1, s_2)$. In the most general case then, the sensor codes s_n are mutually inter-dependent through (3), (4), and (5) according to an implicit relationship.

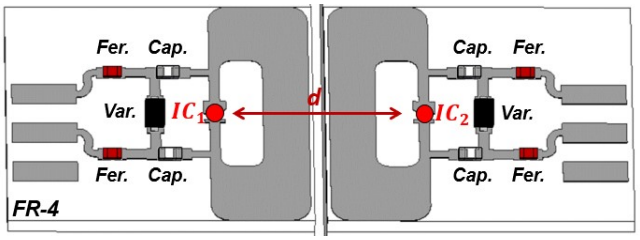

Fig. 3. Layout of the loop trace used in [6] in a dual-chip configuration. Each antenna is on a FR-4 substrate (ε_r= *4.3, tanδ = 0.025, dimensions 14.2×15.1 mm, thickness 1.6 mm)* and the ICs, highlighted in the figure, are placed at a variable distance *d*. Both prototypes lay over a forex substrate (*closed-cell PVC foamboard, ε_r = 1.55, σ= 0.0006 S/m, dimensions 100×50 mm, thickness 5 mm*) not visible in the sketch.

D. Sensitivity matrix

To evaluate the mutual interference between ports, let's introduce the sensitivity matrix $\boldsymbol{\sigma}$:

$$\boldsymbol{\sigma} = \begin{bmatrix} \sigma_{11} & \sigma_{12} \\ \sigma_{21} & \sigma_{22} \end{bmatrix} = \begin{bmatrix} \frac{ds_1}{dC_{S,1}} & \frac{ds_1}{dC_{S,2}} \\ \frac{ds_2}{dC_{S,1}} & \frac{ds_2}{dC_{S,2}} \end{bmatrix} \tag{6}$$

where the main diagonal shows the output variations with respect to the self input variations, and the cross diagonal terms instead represent the output variations with respect to the mutual input variations.

By definition, the sensitivity matrix will depend on the arrangement among antennas, namely on the electromagnetic coupling. In particular, when the two antennas are decoupled, the terms on the cross diagonal are expected to be negligible.

E. Iterative model

Due to the entangled relationship of $B_n^{in}(\Psi) = Im\left[Y_n^{in}\right] = f(\Psi_1, \Psi_2, s_1, s_2)$, the sensor codes $[s_1, s_2]$ can be computed out of the implicit expression (3) by using an iteration method based on the fixed point. We will assume a starting guess for s_1, s_2 equal to an arbitrary value $S_{min} \leq s_0 \leq S_{max}$.

For a fixed set of physical parameters $\boldsymbol{\Psi}$, the iterative method is described next:

1) *k=0;*
2) $s_1^{(k)} = s_2^{(k)} = s_0$;
3) $B_{IC,n}^{(k)} = \omega C_{IC}(s_n^{(k)}) = \omega\left(C_{IC,0} + s_n^{(k)} C_{IC,step}\right)$, *n=1,2;*
4) $Y_{IC,n}^{(k)} = G_{IC,n} + jB_{IC,n}^{(k)}$, *n=1,2;*
5) $\mathbf{Y_G^{(k)}} = \mathbf{Y^{(k)}} + \mathbf{Y_{C_{S,n}}} + \mathbf{Y_{IC,n}^{(k)}} + \mathbf{Y_{C_{S,n}}}(\psi_n)$, *n=1,2;*
6) $Y_n^{in(k)} = \sum_{m=1}^{2} Y_{nm} \frac{\left[\mathbf{Y_G^{-1}}\right]_m \cdot \boldsymbol{g}}{\left[\mathbf{Y_G^{-1}}\right]_n \cdot \boldsymbol{g}}$, *n=1,2;*
7) $B_n^{in(k)} = Im\left[Y_n^{in(k)}\right]$, *n=1,2;*
8) $s_n^{(k+1)} = S_{min} + nint\left(\frac{-1}{C_{IC,step}}\left(C_{IC}(S_{min}) + \frac{B_{in,n}^{(k)}}{\omega}\right)\right)$, *n=1,2;*
9) If $\left|s_n^{(k+1)} - s_n^{(k)}\right| \geq \delta$, then *k=k+1* go back to 3);
10) If $\left|s_n^{(k+1)} - s_n^{(k)}\right| < \delta$, then finish.

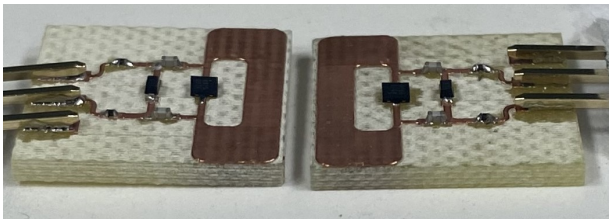

Fig. 4. Prototype of the designed device: two PCBs hosting the loop antennas with all the electronic components and the connectors for the voltage supply.

III. Method Validation

A. Implementation and numerical analysis

The method is here exploited by application to two loop antennas with the same geometry and materials used in [6]. The sensing capacitances $C_{S,n}$ are implemented by two SMV1405 varactor diodes ([11], [12]) so that the capacitance can be modified by a DC voltage supply, emulating the parameter $\boldsymbol{\Psi}$ to be measured.

The considered IC is the Axzon Magnus-S3 [13], with parameters $C_{IC,0} = 1.9pF$, $C_{IC,step} = 3.1\,fF$, conductivity $G_{IC} = 0.482\,mS$, $S_{min} = 80$, $S_{max} = 400$, and nominal power sensitivity $p_{IC} = -16.6\,dBm$.

A symmetrical dual antenna configuration was analyzed and implemented in *CST Microwave Studio Suite 2023* (Fig. 3) at the working frequency of 868 MHz. The sensitivity matrix was evaluated for different arrangement of the two antennas, namely variable:

1) *mutual distance:* the loops were placed in the same working plane in a mirrored configuration and the distance *d* was varyied;
2) *orientation:* the loops were rotated or overlapped to obtain different coupling conditions.

An example of sensitivity matrix for two distances $d = \{62\,mm, 13\,mm\}$ between the loops, and a case in which they are overlapped $(d = 0\,mm)$ are reported next for the fixed values of sensing capacitances $C_S = \{1.2\,pF, 2.1\,pF\}$:

$$\sigma_{(d=62\,mm)} = \begin{bmatrix} 127 & 0 \\ 0 & 127 \end{bmatrix}, \sigma_{(d=13\,mm)} = \begin{bmatrix} 125 & 0 \\ 0 & 125 \end{bmatrix},$$

$$\sigma_{(d=0\,mm)} = \begin{bmatrix} 86 & 37 \\ 68 & 54 \end{bmatrix}.$$

Numerical results show that in the case of decoupled antennas, the sensitivity matrix is symmetrical and diagonal because the cross-sensitivity is equal to zero, as expected.

B. Measurements

The same arrangements as before were experimentally reproduced by using the prototype shown in Fig. 4. The experimental set-up comprised: *i)* a voltage generator to emulate the potentiometric input at one side and *ii)* the PicoScope 2000 oscilloscope [14] at the other side, *iii)* the Keonn circularly polarized Advantenna-p11 [15] for interrogation (Fig. 5), and *iv)* the RadioScan Kit software for sensor code evaluation.

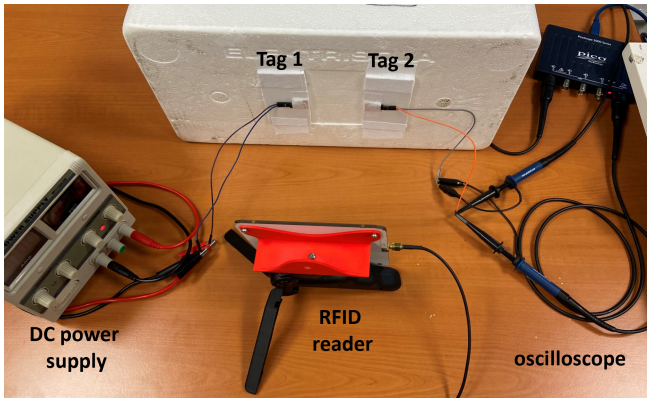

Fig. 5. Experimental setup with a DC power supply and oscillocope as voltage sources, and the Keonn RFID reader interrogating the prototypes under test.

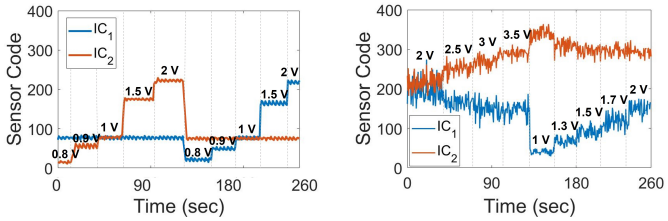

Fig. 6. Sensor codes versus time in a a) decoupled (*d=62 mm*) and b) coupled (*d=0 mm*) dual-sensor configuration.

Fig. 6 shows some preliminary measurements in the case of decoupled and coupled devices. In both the reported configurations, the step voltage was firstly increased at one device while leaving the other fixed, and then vice versa. Where the voltage is not indicated, it was not varied anymore. In the case of decoupled devices (*d=62 mm*), the output signal is much cleaner and less oscillatory, with a medium standard deviation of 3,5 versus 14,5 for the coupled case (*d=0 mm*). Fig. 6 b) shows that, despite one of the two devices being alternatively biased with a constant voltage, the sensor code does not remain stable due to coupling effects.

With reference to Fig. 6, the sensitivity matrix was evaluated in both the decoupled and coupled cases, showing a reasonable agreement with the simulation results:

$$\sigma_{(d=62\,mm)} = \begin{bmatrix} 164.2 & 0 \\ 0 & 172.1 \end{bmatrix},$$

$$\sigma_{(d=0\,mm)} = \begin{bmatrix} 52 & 45 \\ 51 & 114 \end{bmatrix}.$$

For comparison, we refer to a range of 1 V and thus a variable capacitance difference of nearly 1 pF for both matrices.

IV. Conclusions

A method to evaluate the cross-sensitivity of closely coupled capacitive/potentiometric RFID sensors based on auto-tuning microchips has been developed, numerically analyzed, and experimentally verified. Preliminary findings indicate that the dual system configurations exhibit minimal cross-sensitivity, even in case of a few centimeters distance among antennas, except when the antennas partially overlap, leading in this case to significant measurement instability. Moving forward, we plan to expand the formulation to a generic number of ICs and antennas as well as to verify other configurations.

References

[1] C. Wang, M. Liu, Z. Wang, S. Li, Y. Deng, and N. He, "Point-of-care diagnostics for infectious diseases: From methods to devices," *Nano Today*, vol. 37, p. 101092, 2021.

[2] H. Teymourian, C. Moonla, F. Tehrani, E. Vargas, R. Aghavali, A. Barfidokht, T. Tangkuaram, P. P. Mercier, E. Dassau, and J. Wang, "Microneedle-based detection of ketone bodies along with glucose and lactate: toward real-time continuous interstitial fluid monitoring of diabetic ketosis and ketoacidosis," *Analytical chemistry*, vol. 92, no. 2, pp. 2291–2300, 2019.

[3] C. Miozzi, S. Nappi, S. Amendola, C. Occhiuzzi, and G. Marrocco, "A general-purpose configurable rfid epidermal board with a two-way discrete impedance tuning," *IEEE Antennas and Wireless Propagation Letters*, vol. 18, no. 4, pp. 684–687, 2019.

[4] F. Costa, S. Genovesi, M. Borgese, A. Michel, F. A. Dicandia, and G. Manara, "A review of rfid sensors, the new frontier of internet of things," *Sensors*, vol. 21, no. 9, p. 3138, 2021.

[5] P. Yang, J. Wang, H. Chen, Y. Li, W. Jiang, Y. Jing, R. Luo, and S. Qu, "Reducing cross-talk between two patch antennas using integrated electric metamaterials," in *2019 IEEE 2nd International Conference on Electronic Information and Communication Technology (ICEICT)*. IEEE, 2019, pp. 682–685.

[6] F. Nanni and G. Marrocco, "Constrained design of potentiometric rfid sensors based on auto-tuning ics," *IEEE Sensors Journal*, vol. 23, no. 3, pp. 3050–3058, 2022.

[7] N. Panunzio and G. Marrocco, "A multi-port formulation for electromagnetic coupled auto-tuning rfid antennas," in *2021 XXXIVth General Assembly and Scientific Symposium of the International Union of Radio Science (URSI GASS)*. IEEE, 2021, pp. 1–4.

[8] M. C. Caccami and G. Marrocco, "Electromagnetic modeling of self-tuning rfid sensor antennas in linear and nonlinear regimes," *IEEE Transactions on Antennas and Propagation*, vol. 66, no. 6, pp. 2779–2787, 2018.

[9] G. M. Bianco, S. Amendola, and G. Marrocco, "Near-field constrained design for self-tuning uhf-rfid antennas," *IEEE Transactions on Antennas and Propagation*, vol. 68, no. 10, pp. 6906–6911, 2020.

[10] G. Marrocco, "Rfid grids: Part i-electromagnetic theory," *IEEE Transactions on Antennas and Propagation*, vol. 59, no. 3, pp. 1019–1026, 2011.

[11] Skyworks, "SMV1405 to SMV1430 Series - Plastic Packaged Abrupt Junction Tuning Varactors Datasheet," www.skyworksinc.com.

[12] Skyworks - Application Note, "Varactor SPICE Models for RF VCO Applications," www.skyworksinc.com.

[13] Axzon, "RRFM3300-E Magnus-S3 M3E passive sensor IC," https://axzon.com/rfm3300-e-magnus-s3-m3e-passive-sensor-ic/, September 2021.

[14] PicoScope, "Picoscope 2000 series datasheet," https://www.picotech.com/oscilloscope/2000/picoscope-2000-manuals.

[15] Keonn, "Advantenna-p11 rfid uhf wide beam antenna datasheet," https://keonn.com/components-product/advantenna-p11/.